

Two Microwave Land Emissivity Parameterizations Suitable for AMSU Observations

Fatima Karbou

Abstract—In this work, two microwave emissivity parameterizations are proposed to estimate the land emissivity at Advanced Microwave Sounding Units (AMSU) frequencies and scanning conditions in order to help processing AMSU measurements over land surfaces. Both parameterizations are derived from previously calculated land emissivities directly from satellite observations and take into account different surface types from bare soil to areas with high vegetation density. The first parameterization uses best-fit functions derived from February 2000 observations whereas the second parameterization is based on the first one with the addition of a mean nadir emissivity map at 23.8 GHz to allow a more precise surface description. The emissivity parameterizations have been evaluated by comparing emissivity and Tb simulations to target emissivity and Tb observations.

Index Terms—Advanced Microwave Sounding Units (AMSU), microwave surface emissivity, parameterization.

I. INTRODUCTION

THE Advanced Microwave Sounding Units (AMSU) A and B, onboard the latest generation of the National Oceanic and Atmospheric Administration (NOAA) polar-orbiting satellites, offer unique capabilities to monitor the atmospheric temperature and humidity distributions at a global scale. Indeed, AMSU-A benefits from channels near the 50–60-GHz oxygen absorption band and is able to retrieve atmospheric temperature profiles from about 45 km down to the Earth's surface. AMSU-B channels, located in the vicinity of the strong water vapor absorption line at 183.31 GHz, measure the thermal emission of water vapor arising from different atmospheric layers. In addition, the two instruments provide measurements from window channels (23.8, 31.4, 50.3, 89, and 150 GHz) that are mainly sensitive to surface and low atmospheric effects.

So far, the AMSU profiling information is still more intensively exploited over ocean than over land, in spite of ongoing efforts made in many operational numerical weather prediction (NWP) centers [5], [7], [24]. Only channels that are not contaminated by the surface are assimilated, but accurate land emissivities are also needed to extend the use of AMSU observations to include channels more sensitive to the surface. Atmospheric retrievals over land are more difficult to perform because the surface contribution to the measured radiation is important due to higher emissivity values over land than over ocean. In addition, the land emissivity is difficult to model and is associated with

rather high temporal and spatial variations with surface types, roughness, and moisture content, among other parameters.

According to English [4], the land emissivity has to be estimated within 2% for effective atmospheric humidity profile retrievals over continental surfaces. Prigent *et al.* [28], and more recently Karbou *et al.* [16], have shown that the land emissivity can be estimated from remotely sensed microwave observations with a day-to-day variability within 2% over a variety of surface types, and for different observation angles and frequencies. Then, based on emissivity calculations directly derived from satellite AMSU window channels together with accurate skin temperature estimations, the potential of AMSU-A and -B measurements for atmospheric temperature and humidity profiling over land has been studied [17].

In addition to estimating surface emissivity from microwave satellite observations (see [2], [6], [15], [16], [21], [22], [24], [27], [28] among others), other emissivity studies were carried out, using ground-based measurements [1], [18], [19], [32] and aircraft observations [11], [12]. Moreover, different models have been developed (e.g., see [10], [14], and [31]) to simulate microwave emissivity spectra for different surface conditions. However, the modeling approaches for global applications are mainly limited by the lack of accurate input parameters necessary to feed the model (vegetation characteristics, soil moisture, and roughness, among others).

This study aims to present two parameterizations of the microwave land emissivity, anchored on emissivities directly derived from satellite observations, useful to process AMSU data over land. This work is motivated by the need to develop a practical procedure to determine the microwave land emissivity suitable for AMSU observations which can be easily implemented into the NWP models. Previously derived emissivities from AMSU observations vary with the observation angle, the frequency, as well as the surface type [16]. For instance, there is a strong angular dependence of the AMSU emissivity over bare soils whereas it is negligible over forested land. The direct use of the already calculated AMSU emissivity atlas for atmospheric applications is mainly hampered by the need to produce mean emissivity maps at different zenith angles to account for the angular variation of AMSU emissivities. However, unlike conical instruments, the cross-track scanning pattern of AMSU has, as a consequence of it, a limited number of observations per scan position especially during year 2000 when only NOAA-15 satellite was operational.

The AMSU observations and emissivity datasets are described in Section II. The microwave emissivity parameterization is presented in Section III. Two complementary parameterization approaches are discussed in the later section, and their results are evaluated using five months of data in Section IV. General conclusions are provided in Section V.

Manuscript received September 30, 2004; revised April 26, 2005.

The author was with the Centre National de la Recherche Scientifique (CNRS), Centre d'étude des Environnements Terrestre et Planétaires (CETP), 78140, Vélizy, France. She is now with the CNRS, Centre National de Recherches Météorologiques (CNRM), Météo-France, 31057, Toulouse Cedex 1, France (e-mail: fatima.karbou@cnrm.meteo.fr).

Digital Object Identifier 10.1109/TGRS.2005.851168

TABLE I
AMSU-A/B CHANNEL CHARACTERISTICS

Channel No	Frequency (GHz)	Noise equivalent (K)	Resolution at nadir (km)
AMSU-A			
1	23.8	0.20	48
2	31.4	0.27	48
3	50.3	0.22	48
4	52.8	0.15	48
5	53.596+/- 0.115	0.15	48
6	54.4	0.13	48
7	54.9	0.14	48
8	55.5	0.14	48
9	57.290=f ₀	0.20	48
10	f ₀ +/- 0.217	0.22	48
11	f ₀ +/- 0.322 +/- 0.048	0.24	48
12	f ₀ +/- 0.322 +/- 0.022	0.35	48
13	f ₀ +/- 0.322 +/- 0.010	0.47	48
14	f ₀ +/- 0.322 +/- 0.0045	0.78	48
15	89	0.11	48
AMSU-B			
16	89	0.37	16
17	150	0.84	16
18	183.31 +/- 1	1.06	16
19	183.31 +/- 3	0.70	16
20	183.31 +/- 7	0.60	16

II. AMSU AND EMISSIVITY DATASETS

A. AMSU Data

The AMSU-A and -B soundings units are operational on board the latest generation of polar orbiting satellites NOAA-15, -16, -17, and recently onboard the Aqua satellite. AMSU-A, designed for atmospheric temperature retrieval, measures the outgoing radiation from the Earth's surface and from different atmospheric layers using 15 spectral regions (23.8–89.0 GHz). AMSU-B is designed for humidity sounding and has two window channels at 89 and 150 GHz and three other channels centered on the 183.31-GHz water vapor line. AMSU-A and -B have a nominal field of view of 3.3° and 1.1° and sample 30 and 90 Earth views, respectively. Thereby, the AMSU observation scan angle varies up to 48° which translates into 58° of local zenith angle. Channel characteristics for both AMSU-A and AMSU-B radiometers are given in Table I, and detailed description of the AMSU sounders is reported in [8].

In this study, the level 1b AMSU data from January to August 2000 have been obtained from the Satellite Active Archive (SAA) and then processed using the Advanced ATOVS Processing Package (AAPP) created and distributed by the European Organization for the exploitation of Meteorological satellites (EUMETSAT) and other partners. For the present analysis, we focus on a large geographic area (from 60°W to 60°E in longitude and from 60°S to 60°N in latitude) to include wide ranges of surface conditions. The AMSU radiances were corrected for the AMSU antenna effect [13], [20].

Compared to infrared sounding measurements, AMSU observations are less sensitive to high thin and nonprecipitating clouds. However, only cloud-free data have been selected for an optimum accuracy of the emissivity estimates. The cloud screening is conducted using the International Satellite Cloud Climatology Project (ISCCP) DX datasets. Cloud parameters and skin temperatures are extracted from ISCCP every 30 km and every 3 h. In the ISCCP processing, information about clouds is obtained from visible and infrared measurements from polar and geostationary satellites, using radiative analysis [29].

B. AMSU Land Emissivity

The AMSU land surface emissivities have been estimated using data from year 2000, for 30 observation zenith angle ranges (from -58° to +58°) and for the 23.8-, 31.4-, 50.3-, 89-, and 150-GHz channels [16]. Collocated visible/infrared satellite measurements from ISCCP data have been used to screen for cloud and rain effects and to provide an accurate estimate of the skin temperature. The nearby temperature-humidity profiles from ECMWF 45-year reanalyses (ERA-40) [33] have been used as inputs to a up-to-date microwave radiative transfer model [23] in order to estimate the atmospheric contribution to the measured radiances. The AMSU emissivities have been estimated under the assumption of a flat and specular surface. Because of the rotating AMSU antenna, the estimated emissivity is a mixture between emissivities in the vertical and the horizontal polarizations. The AMSU emissivity at scan angle θ_{SCAN} can be written as follows:

$$\varepsilon(\theta_{ZEN}) = \varepsilon_V(\theta_{ZEN}) \times \cos^2(\theta_{SCAN}) + \varepsilon_H(\theta_{ZEN}) \times \sin^2(\theta_{SCAN}) \quad (1)$$

where $\varepsilon_H(\theta_{ZEN})$ and $\varepsilon_V(\theta_{ZEN})$ are emissivities in the horizontal and vertical polarizations, respectively.

The consistency of the estimated AMSU emissivities has been checked by analyzing their dependencies with surface types, observation angles, and frequencies [16]. The AMSU emissivities have been further evaluated by comparison with the previously calculated SSM/I ones [28]. A very good agreement between the two emissivity datasets has been found. AMSU emissivities have been sorted out by surface type, using the Biosphere-Atmosphere Transfer Scheme (BATS) land-cover classification [3]. Table II lists the used land-cover classes. Monthly mean emissivity maps (not presented) show the natural changes of the emissivity, mainly related to changes in surface types. For example, lakes and rivers as well as the coastlines are associated with low emissivities at all frequencies but also with high emissivity horizontal variability. For the entire datasets, the day-to-day emissivity standard deviations are generally less than 2% for AMSU surface channels and tend to increase with

TABLE II
BIOSPHERE-ATMOSPHERE TRANSFER SCHEME (BATS) LAND COVER CLASSES

Classes	Legend
1	Crops, Mixed Farming
2	Short Grass
3	Evergreen Needleleaf Trees
4	Deciduous Needleleaf Tree
5	Deciduous Broadleaf Trees
6	Evergreen Broadleaf Trees
7	Tall Grass
8	Desert
9	Tundra
10	Irrigated Crops
11	Semi-desert
12	Ice Caps and Glaciers
13	Bogs and Marshes
14	Inland Water
16	Evergreen Shrubs
17	Deciduous Shrubs
18	Mixed Forest
19	Interrupted Forest
20	Water and Land Mixtures

the frequency and the zenith angle. The angular dependence of the estimated AMSU emissivities is found to be important over bare soil areas, and limited over dense vegetation areas. Fig. 1 illustrates the monthly mean emissivity variation with scan position (i.e., zenith angle) at 23.8, 31.4, 50.3, and 89 GHz over a six-month period, and both desert and dense vegetation areas. This figure also shows that the emissivity curves with respect to surface type and scan position, have similar trends for the whole period. Additional analysis, involving other surface types, gives similar results. Consequently, given a surface type and a frequency, the remarkable stable pattern of the emissivity variation with the scan position (indirectly with the observation zenith angle) can be used to derive a microwave land emissivity parameterization.

It should be mentioned that a scan asymmetry, relatively to nadir, has been highlighted by analyzing the AMSU emissivity angular dependency. This asymmetry was also noticed by Weng *et al.* [30] and is probably related to an instrumental problem. The scan asymmetry is found to be variable with frequency and surface emissivity, with a maximum scan bias (difference between the emissivities at scan positions 1 and 30) at 31.4 GHz (almost 3%) and at 23.8 GHz (2.4%) over bare soil areas [16].

III. TWO EMISSIVITY PARAMETERIZATIONS DERIVED FROM AMSU EMISSIVITY ESTIMATES

A. First Parameterization

As seen earlier (Section II-B), mean emissivity curves sorted by scan position and surface type show remarkably month-to-month stable patterns. This property is very interesting because it means that it is possible to characterize each surface type by a function that describes the emissivity angular and frequency variations. It also means that, at a first stage, a one month period of emissivity estimations can be sufficient to derive such functions.

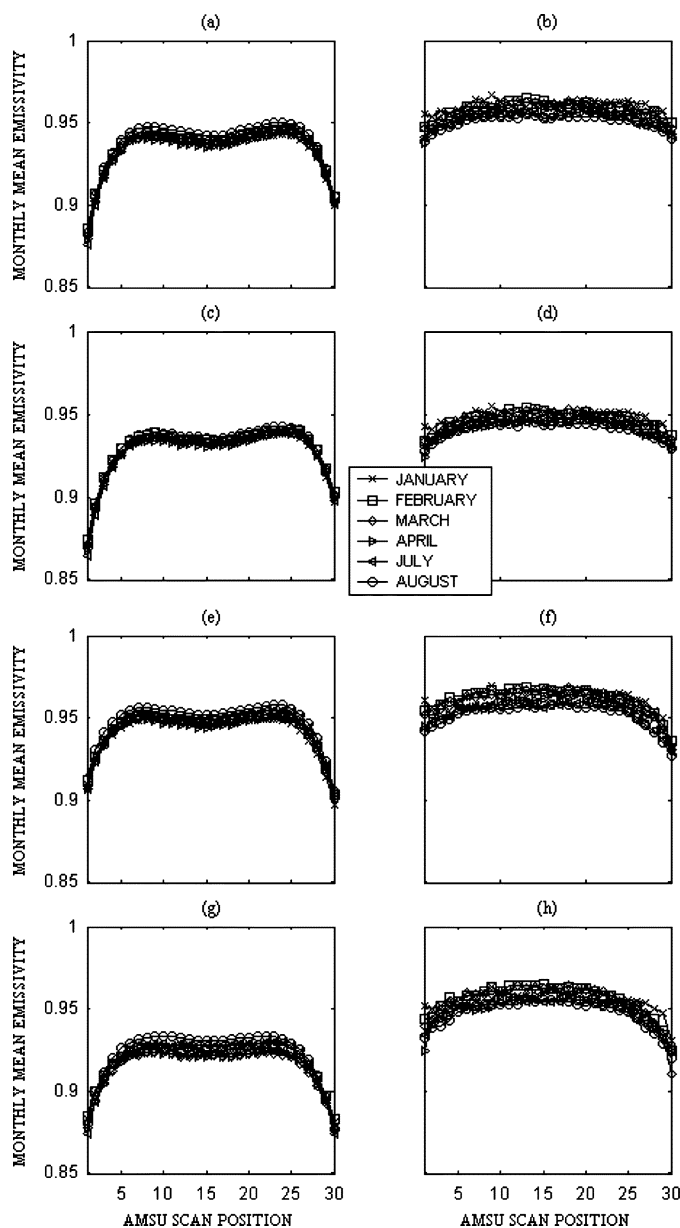


Fig. 1. Monthly mean AMSU emissivities for January, February, March, April, July, and August 2000 with respect to 30 scan positions ($\pm 58^\circ$ of zenith angle variation). Scan positions 15 and 16 correspond to nadir and at 23.8-, 31.4-, 50.3-, and 89-GHz frequencies over both desert and dense vegetation areas. (a) Desert at 23.8 GHz. (b) Dense vegetation at 23.8 GHz. (c) Desert at 31.4 GHz. (d) Dense vegetation at 31.4 GHz. (e) Desert at 50.3 GHz. (f) Dense vegetation at 50.3 GHz. (g) Desert at 89 GHz. (h) Dense vegetation at 89 GHz.

Emissivity estimates from February 2000 have been chosen to derive the first emissivity parameterization based on fit functions that best represent emissivity variation per scan position, frequency and surface type. For all surface types, polynomial fit functions of degree 5 are found appropriate to fit emissivity data. Given a land-cover class, the best-fit emissivity function can be expressed according to the frequency and the scan position as follows:

$$E_{(v,FOV)} = P_v^1 \times (FOV - 15)^5 + P_v^2 \times (FOV - 15)^4 + P_v^3 \times (FOV - 15)^3 + P_v^4 \times (FOV - 15)^2 + P_v^5 \times (FOV - 15)^1 + P_v^6 \quad (2)$$

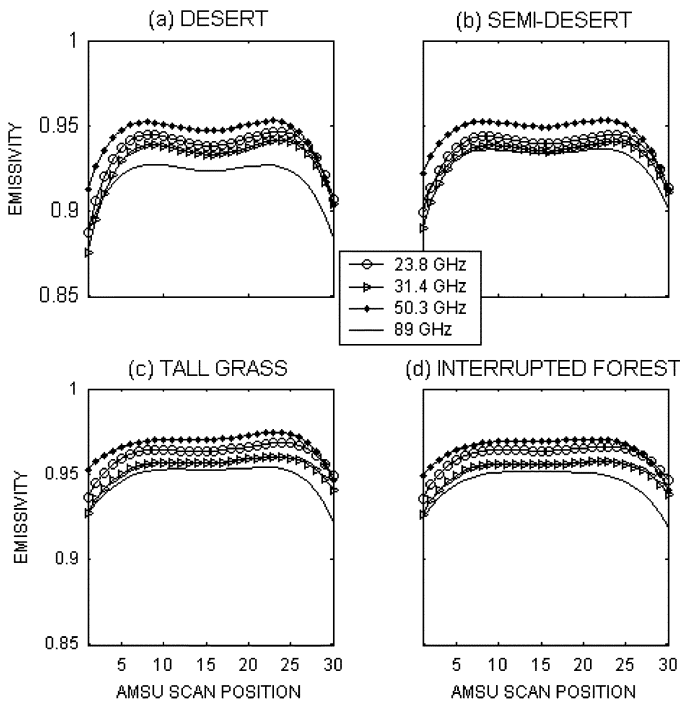


Fig. 2. Emissivity best-fit functions with respect to 30 scan positions ($\pm 58^\circ$ of zenith angle variation) at 23.8-, 31.4-, 50.3-, and 89-GHz frequencies and over (a) desert, (b) semidesert, (c) tall grass, and (d) interrupted forest areas.

where $E_{(v,FOV)}$ is the best-fit emissivity function at frequency v and scan position FOV. It is worthy to note that AMSU-A scan position varies from 1 to 30, which translate into $\pm 58^\circ$ zenith angle variation (scan positions 15 and 16 correspond to nadir observation). $P_v^1, P_v^2, P_v^3, P_v^4, P_v^5,$ and P_v^6 are the polynomial fit coefficients for frequency v , with $v = 23.8, 31.4, 50.3, 89,$ and 150 GHz. One could note that the P_v^6 coefficient represents the nadir emissivity for frequency v .

Fig. 2, shows the obtained best-fit emissivity curves for dry (vegetation cover 8 and 11) and vegetated (vegetation cover 7 and 19) areas with respect to the AMSU-A scan position using the parameterization coefficients described earlier. For a given AMSU observation, and using the present parameterization, we can simulate the corresponding land emissivity by: 1) identifying the surface type using the observation geographic location (latitude/longitude) and then 2) using (2), the emissivity can be computed according to the observation scan position and frequency.

Emissivity simulations for August 2000 have been performed following this method and have been compared to target emissivities directly calculated from satellite measurements (see Section II-B). So far, there are no extensive *in situ* emissivity measurements that can be reliably compared with the simulated emissivities. Moreover, the direct AMSU emissivity calculations have been carefully evaluated by looking at their frequency and angular dependencies, and also by comparing them to other emissivity datasets. Fig. 3(a) shows the mean August 2000 emissivity map at 31.4 GHz directly calculated from satellite observations (from [16]) whereas Fig. 3(b) shows the mean bias between the calculated and the simulated emissivities using the parameterization method described

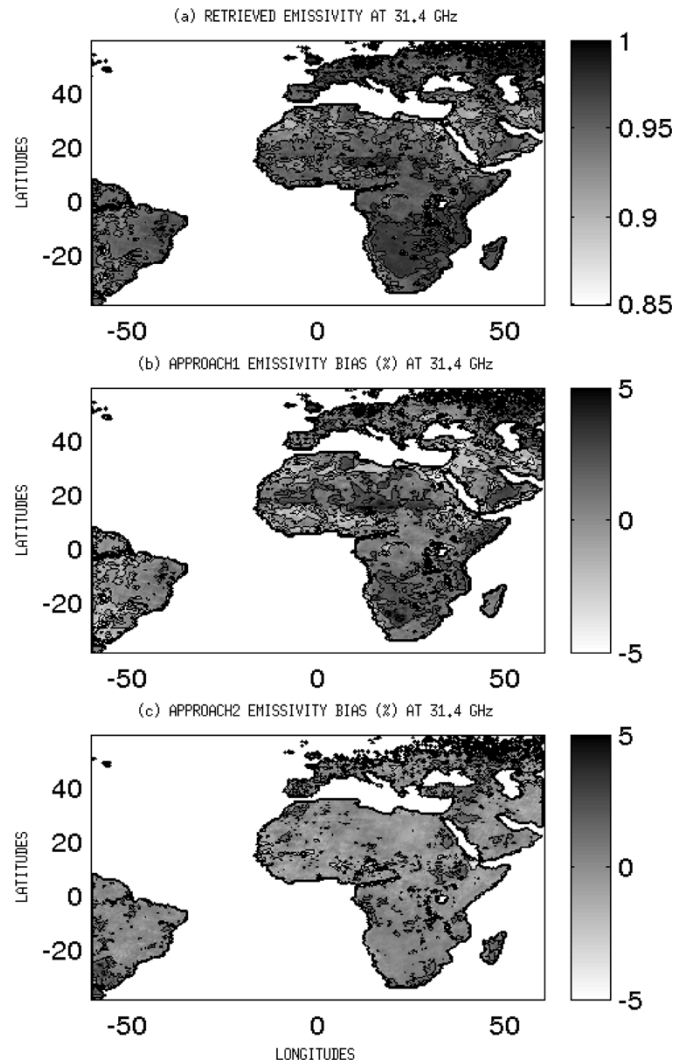


Fig. 3. Monthly mean maps obtained at 31.4 GHz and all zenith angles using data from August 2000. (a) Mean emissivity map directly derived from satellite observations. (b) Mean emissivity bias map in percent between the calculated and the simulated emissivity using the first parameterization. (c) Mean emissivity bias map in percent between the calculated and the simulated emissivity using the second emissivity parameterization.

earlier. AMSU-A observations at all zenith angles were used to plot these maps. Lakes and rivers show larger emissivity bias (see for instance the Congo river and the Nile) as well as the coastlines. Some locations in the Arabian plate and in North Africa show also high biases. Most of these regions are defined as desert surface and therefore has one best-fit function to calculate the emissivity. It is clear that, within this region, we need a more detailed land-cover classification to correctly account for the natural variation of the emissivity. For vegetated areas, the parameterization provides emissivity simulations in good agreement with the target emissivities. In addition, similar geographic patterns can be observed in both subplots 3(a) and (b). For example, in the desert, two particular areas of very low emissivities and high emissivity biases are observed, one, in the South of Arabia (Western Oman, Eastern Yemen) and another one, in Egypt. These microwave signatures are probably related to very specific geological structures [25].

The first emissivity parameterization is a compromise that allows one to process data over land. However, this parameterization has many limitations: first, it does not account for open water (rivers, lakes, coastlines) and relief areas. Second, the intrinsic emissivity variability within a specific land-cover class is also neglected; the desert for example has to be more precisely described in order to better account for it in the emissivity parameterization. Finally, the seasonal variation of the emissivity is not accounted for.

B. Second Parameterization

In order to better account for the natural variation of the emissivity with surface types, a second parameterization is developed. This approach is based on the first one with the addition of a mean monthly nadir emissivity map at 23.8 GHz and from July 2000. A mean summer emissivity map is chosen to limit the rain-induced soil moisture emissivity contamination. However, even for July data, the potential of cloud contamination is likely to occur. Moreover, the subsahelian transition zone in Africa experiences rain-induced soil moisture variations. For a given AMSU observation and according to the second parameterization, we can simulate the corresponding land emissivity as follows.

- Step 1) We identify the surface type using the observation geographic location (latitude/longitude).
- Step 2) Then from the mean nadir emissivity map at 23.8 GHz: the closet emissivity value to the observation is assigned to the coefficient $P_{23.8}^6$.
- Step 3) Previous studies [2], [15], [16], [26] have shown that for most surfaces, the microwave emissivity varies smoothly with the frequency. Consequently, the remaining P_v^6 coefficients with $v = 31.4, 50.3, 89,$ and 150 GHz can be updated using a linear formula

$$P_v^6 = P_{23.8}^6 + P_v^6 - P_{23.8}^6 \quad (3)$$

where P_v^6 are the first parameterization coefficients and P_v^6 are the updated ones.

- Step 4) Once P_v^6 coefficients are updated, the emissivity can be computed from (2) according to the observation scan position and frequency.

Emissivity simulations using the second parameterization are compared to target emissivities directly computed from satellite observations [subplot 3(c)]. Contrary to the first approach, the second one gives a better account of the natural variation of the emissivity within the study area. The emissivity biases between the retrieved and the simulated emissivities are now within 1% in most regions and for all observation zenith angles. Even lakes and rivers are now characterized by low emissivity biases.

In the following section, we will further evaluate both emissivity parameterizations by comparing brightness temperature (Tb) simulations to Tb observations over land.

IV. EVALUATION OF THE TWO EMISSIVITY PARAMETERIZATIONS

In order to evaluate the proposed microwave emissivity parameterizations, radiative transfer calculations in cloud-free

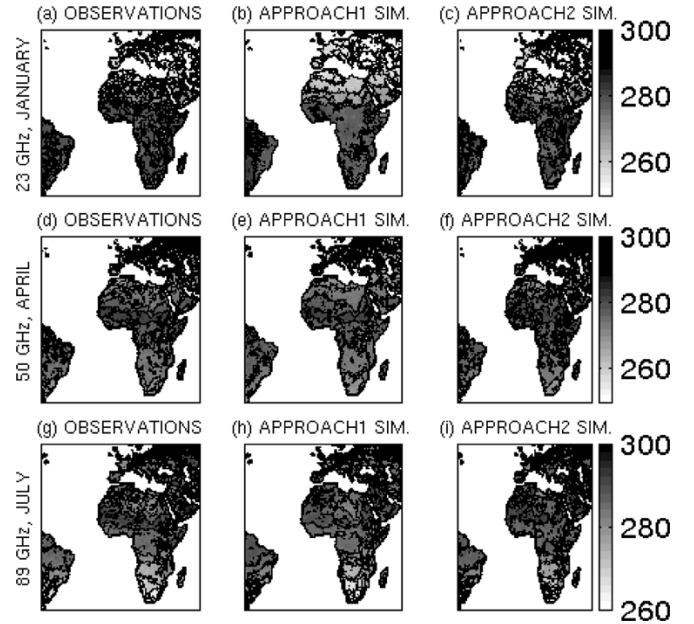


Fig. 4. Monthly mean T_b s maps obtained from (a) all AMSU January observations at 23 GHz, (b) simulations using the first parameterization for the same period and frequency, and (c) simulations using the second parameterization for the same period and frequency. (d), (e), and (f) are same as (a), (b), and (c) but using data from April 2000 at 50.3 GHz. Subplots (g), (h), and (i) are same as (a), (b), and (c) but using data from July 2000 at 89 GHz.

conditions and using five months of data [January, March, April, July (except data from the 23.8-GHz channel) and August 2000] have been performed. The collocated ECMWF temperature and humidity profiles during this period have been used as inputs to an up-to-date radiative transfer model [23] to calculate the cloud-free atmospheric contribution to the measured radiances. ISCCP datasets have been used to screen clouds and to provide skin temperature estimates. The computations are done at all AMSU-A scan positions and at the frequencies 23.8, 31.4, 50.3, and 89 GHz. For a nonscattering plane-parallel atmosphere and, for a given path zenith angle, the brightness temperature (T_b) observed by the satellite instrument can be expressed as

$$Tb_{(v,FOV)} = (T_{skin} \times \varepsilon_{(v,FOV)} \times \Gamma) + (T_{(v,\downarrow)} \times (1 - \varepsilon_{(v,FOV)}) \times \Gamma) + T_{(v,\uparrow)} \quad (4)$$

where $Tb_{(v,FOV)}$ and $\varepsilon_{(v,FOV)}$ are the simulated brightness temperature and emissivity at frequency v and at scan position FOV, respectively, T_{skin} is the ISCCP skin temperature, $T(v, \uparrow)$, $T(v, \downarrow)$, and Γ , are the upwelling, the downwelling brightness temperatures, and the net atmospheric transmissivity, respectively, calculated for the given atmospheric profiles, path zenith angle, and the frequency v using the ATM model [23]. This model is based on different developments and recent measurements, is fully applicable in the 0–1600-GHz frequency range and has been evaluated by intercomparisons with other existing radiative transfer models.

The comparisons between the observed and the simulated T_b s are shown in Fig. 4 for January, April, and July 2000. Subplot 4(a) presents the observed mean T_b s from January at 23 GHz whereas subplots 4(b) and (c) show the simulated mean T_b s for

the same period and frequency using the first and the second parameterizations, respectively. The agreement is best between the observed and the simulated Tbs, over bare soil areas using the second parameterization, because the surface is better described with the help of the mean nadir emissivity map. Indeed, emissivity bias is reduced over the Arabian plateau and over some locations in North Africa. This is confirmed by looking at the Tb difference (observations-simulations) histograms calculated using August 2000 data at window channels over desert surfaces and at 23.8, 31.4, 50.3, and 89 GHz [see subplots 5(a)–(h)]. The histograms are separated by zenith angle ranges [low zenith angles (angles $\leq 20^\circ$) and high zenith angles (angles $> 45^\circ$)]. The Tb simulations have been calculated using: 1) a constant emissivity value (0.95); 2) and 3) emissivities simulated using the first and second emissivity parameterizations, respectively. At all frequencies, the Tb biases and standard deviations are higher when using an emissivity constant value, especially for high zenith angles. Tbs simulated with the second parameterization are in better agreement with the observed Tbs than Tbs simulated with the first parameterization. However, over dense vegetation surfaces (not shown) both emissivity parameterizations give satisfactory Tb simulations. The histograms also show that accurate skin temperatures are necessary but not sufficient, for effective Tb simulations, and that reliable emissivities are important, to correctly estimate the surface contribution to the measured radiances.

Over Eastern Europe, where rain and/or snow contamination is likely during January, we can notice a less precise agreement between observed and simulated Tbs (using both emissivity parameterizations). Actually, the parameterization does not account for rain-induced soil moisture effects and therefore, with a likely rain contamination, both emissivity parameterizations overestimate the emissivity. An emissivity overestimation translates into an increase in the simulated brightness temperature. Moreover, the month-to-month variation of the emissivity is not accounted for, and leads to additional emissivity estimation errors.

Similar comments can be made while looking at results from April 2000 at 50.3 GHz on subplots 4(d)–(f) and results from July 2000 at 89 GHz [subplots 4(g)–(i)]. For a five-month period and for both parameterizations, the agreement between the observed and simulated Tbs is found to be better for low frequencies (23, 31, and 50 GHz) than for higher ones (89 and 150 GHz). The last two channels are more affected by surface and low atmosphere errors than the other channels. It should be noted that, for most surfaces, the AMSU emissivity varies smoothly with frequency and that is possible to extrapolate it at sounding channels from the closest window channels [16]. Consequently, emissivities simulated at discrete window frequencies can be used to process data not only from surface channels but also from the closest sounding channels.

Further Tb comparisons are provided in Fig. 6 with Tb root mean square (RMS) of errors maps calculated for window channels, using the difference between the observed Tbs and the simulated ones, for August data. RMS Tb maps illustrate a good agreement between the observed Tbs and the simulated ones according to the second emissivity parameterization for all window channels, especially at 50 GHz, with less than 3 K

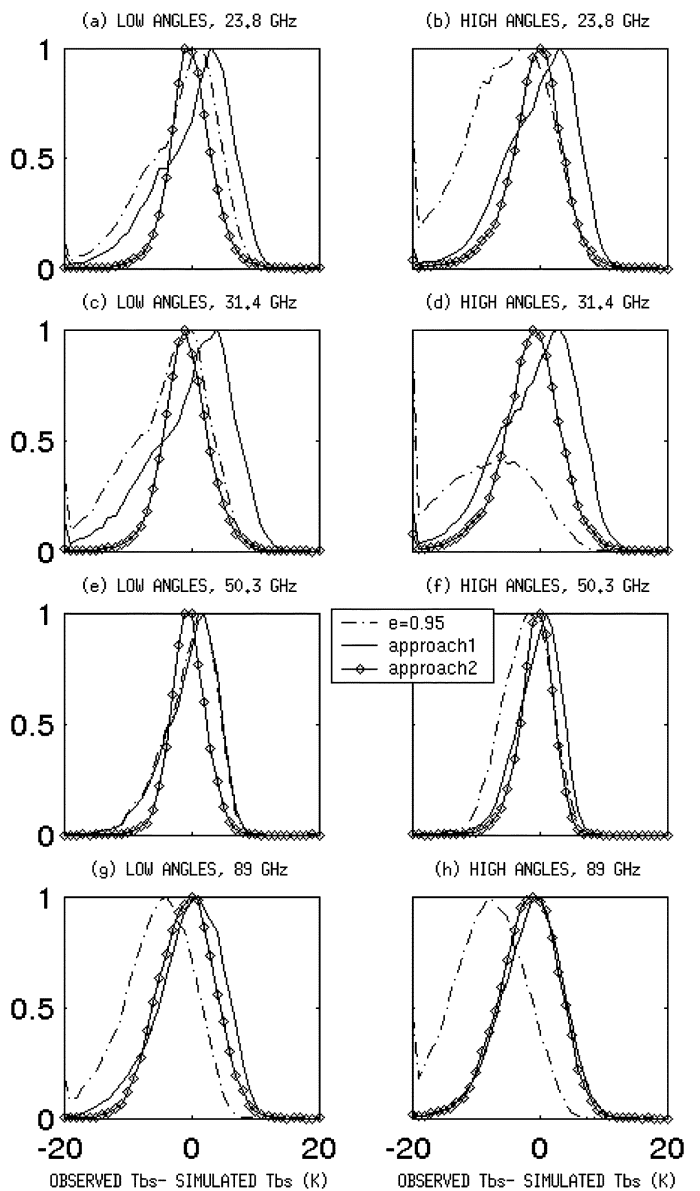


Fig. 5. Histograms of Tbs difference between measurements and simulations over desert using data from August 2000, for (a) 23.8-GHz channel and low angles ($\leq 20^\circ$), (b) 23.8-GHz channel and high angles ($> 40^\circ$). (c) to (h) Same as (a) and (b) but for 31.4, 50.3, and 89 GHz, respectively. Tbs simulations have been performed using: 1) a fixed emissivity (0.95) (dashed-dotted lines); 2) emissivities estimated using the first parameterization (solid lines); and 3) emissivities estimated using the second parameterization (solid line with diamond symbols).

of RMS of errors, for the entire study area. There are still areas with high Tbs RMS mainly relief areas and coastlines where navigation errors are likely to happen.

Compared with the first parameterization, the second one gives better results over areas poorly described in the land-cover classification. However: 1) rain-induced soil moisture effects and snow phenomena are not accounted for (it is difficult to have a precise description of the rain occurrences at global scales) and 2) all seasonal variations of the emissivity due to vegetation cover developments are ignored.

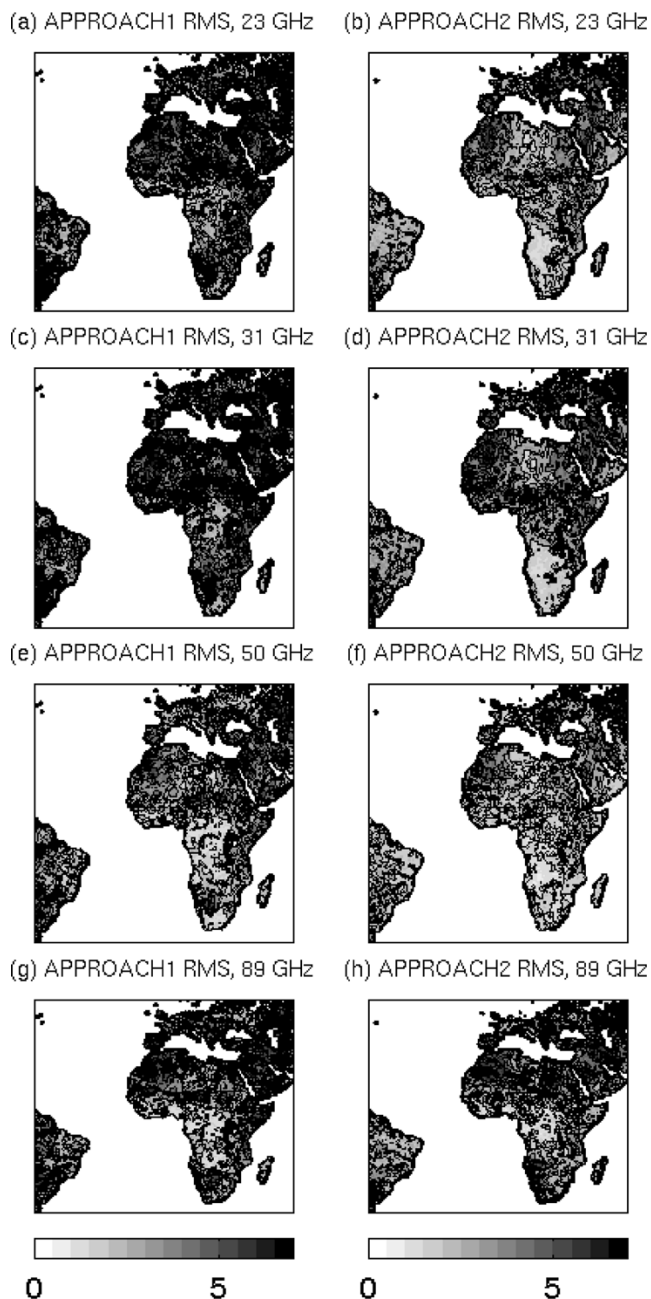


Fig. 6. Monthly RMS of errors maps for August 2000 obtained by calculating the differences between the observed Tbs and (a) the simulated Tbs at 23.8 GHz using the first emissivity parameterization and (b) the simulated Tbs at the same frequency using the second parameterization. Subplots (c) and (d) are similar to (a) and (b) but for the 31.4-GHz channel. Subplots (e) and (f) are similar to (a) and (b) but for the 50.3-GHz channel. Subplots (g) and (h) are similar to (a) and (b) but for the 89-GHz channel.

Both emissivity parameterizations could be optimized if the seasonal variation of the emissivity is taken into account. For instance, one could generate different best-fit emissivity functions by season for the first parameterization or include mean nadir emissivity maps per month for the second parameterization.

V. CONCLUSION

Two parameterizations of the land emissivity useful for frequencies ranging from 23–150 GHz are proposed. Both

emissivity parameterizations are anchored on recent land emissivity calculations directly from AMSU observations. The first one uses best-fit functions derived from February 2000 observations that varies with land-cover surface, frequency and scan position. The second parameterization is based on the first one with the addition of a mean nadir emissivity map at 23.8 GHz to allow a more precise surface description. Both parameterizations have been evaluated by comparing the simulated emissivity to target emissivities directly estimated from satellite measurements. The second parameterization is found to be more accurate than the first one over areas poorly described in the land-cover classification (such as bare soil areas). Over other surfaces, both parameterization results are satisfactory. With the first and the second parameterizations, the results are better at low frequencies (23–50 GHz) than at higher ones (89 and 150 GHz). The emissivity parameterizations have been further evaluated by comparing simulated Tbs to target observed ones for five months of data with similar conclusions. The proposed parameterizations are a compromise to process data from an AMSU like instrument (with the same polarization and scanning conditions such as SSM/T2 sensor) or from AMSU instruments on board different satellite platforms (NOAA16-17 and Aqua).

However, there are still some limitations to the emissivity parameterization for global applications: the emissivity seasonal variations are not accounted for as well as rain/snow effects. Moreover, the proposed parameterizations are based on AMSU data; and therefore are instrument dependent.

ACKNOWLEDGMENT

The author gratefully acknowledges C. Prigent for helpful discussions and suggestions about the manuscript. The author is very grateful to L. Eymard for many constructive suggestions and comments on this work. The author would like to thank J. Maziejewski for his help to revise the manuscript. The author would further like to thank three anonymous reviewers as well as the associate editor for their most constructive comments and valuable suggestions for improving the manuscript. The author wishes to thank J. R. Pardo who kindly provided the ATM radiative transfer model. The ISCCP data have been directly provided by B. Rossow, AMSU data via the SAA and ERA40 from ECMWF. The emissivity best-fit coefficients are available for use by the scientific community and can be obtained by request to the author.

REFERENCES

- [1] J.-C. Calvet, J.-P. Wigneron, A. Chanzy, S. Raju, and L. Laguerre, "Microwave dielectric properties of a silt-loam at high frequencies," *IEEE Trans. Geosci. Remote Sens.*, vol. 33, no. 3, pp. 634–642, May 1995.
- [2] B. J. Choudhury, "Reflectivities of selected land surface types at 19 and 37 GHz from SSM/I observations," *Remote Sens. Environ.*, vol. 46, no. 1, pp. 1–17, 1993.
- [3] R. E. Dickinson, A. Henderson-Sellers, P. J. Kennedy, and M. F. Wilson, "Biosphere-atmosphere transfer scheme (BATS) for the NCAR community climate model," Boulder, CO, NCAR Tech. Note NCAR/TN275+STR, 1986.
- [4] S. English, "Estimation of temperature and humidity profile information from microwave radiances over different surface types," *J. Appl. Meteorol.*, vol. 38, pp. 1526–1541, 1999.

- [5] S. English, F. Hilton, B. Candy, K. Whyte, N. Atkinson, A. Smith, B. Bell, U. O'keeffe, and A. Doherty, "Operational use of ATOVS at the Met Office," presented at the *13th Int. TOVS Study Conf.*, Sainte-Adèle, QC, Canada, 2003.
- [6] G. W. Felde and J. D. Pickle, "Retrieval of 91 and 150 GHz earth surface emissivities," *J. Geophys. Res.*, vol. 100, no. D10, pp. 20 855–20 866, Oct 1995.
- [7] E. Gérard, F. Rabier, D. Lacroix, and Z. Sahlaoui, "Use of ATOVS raw radiances in the operational assimilation system at Météo-France," in *Proc. 13th Int. TOVS Study Conf.*, Sainte-Adèle, QC, Canada, 2003, pp. 18–29.
- [8] G. Goodrum, K. B. Kidwell, and W. Winston, *NOAA KLM User's Guide*. Camp Springs, MD: Nat. Oceanic Atmos. Admin., 2000.
- [9] N. C. Grody, J. Zhao, R. Ferraro, F. Weng, and R. Boers, "Determination of precipitable water and cloud liquid water over oceans from the NOAA-15 advanced microwave sounding unit," *J. Geophys. Res.*, vol. 106, pp. 2943–2954, 2001.
- [10] N. C. Grody, "Surface identification using satellite microwave radiometers," *IEEE Trans. Geosci. Remote Sens.*, vol. 26, no. 6, pp. 850–859, Nov. 1988.
- [11] T. J. Hewison, "Airborne measurements of forest and agricultural land surface emissivity at millimeter wavelengths," *IEEE Trans. Geosci. Remote Sens.*, vol. 39, no. 2, pp. 393–400, Feb. 2001.
- [12] T. J. Hewison and S. English, "Airborne retrieval of snow and ice surface emissivity at millimeter wavelengths," *IEEE Trans. Geosci. Remote Sens.*, vol. 37, no. 4, pp. 1871–1879, Jul. 1999.
- [13] T. J. Hewison and R. W. Saunders, "Measurements of the AMSU-B antenna pattern," *IEEE Trans. Geosci. Remote Sens.*, vol. 34, no. 2, pp. 405–412, Mar. 1996.
- [14] R. G. Isaacs, Y.-Q. Jin, R. D. Worsham, G. Deblonde, and V. J. Falcone, "The RADTRAN microwave surface emission models," *IEEE Trans. Geosci. Remote Sens.*, vol. 27, no. 4, pp. 433–440, Jul. 1989.
- [15] A. S. Jones and T. H. Vonder Haar, "Retrieval of microwave surface emittance over land using coincident microwave and infrared satellite measurements," *J. Geophys. Res.*, vol. 102, no. D12, pp. 13 609–13 626, Jun. 1997.
- [16] F. Karbou, C. Prigent, L. Eymard, and J. R. Pardo, "Microwave land emissivity calculations using AMSU measurements," *IEEE Trans. Geosci. Remote Sens.*, vol. 43, no. 5, pp. 948–959, May 2005.
- [17] F. Karbou, F. Aires, C. Prigent, and L. Eymard, "Potential of Advanced Microwave Sounding Unit-A (AMSU-A) and AMSU-B measurements for temperature and humidity sounding over land," *J. Geophys. Res.*, vol. 110, no. D07109, 2005. DOI:10.1029/2004JD005318.
- [18] C. Mazler, "Passive microwave signatures of landscapes in winter," *Meteorol. Atmos. Phys.*, vol. 54, pp. 241–260, 1994.
- [19] —, "Seasonal evolution of microwave radiation from an oat field," *Remote Sens. Environ.*, vol. 31, pp. 161–173, 1990.
- [20] T. Mo, "AMSU-A antenna pattern corrections," *IEEE Trans. Geosci. Remote Sens.*, vol. 37, no. 1, pp. 103–112, Jan. 1999.
- [21] J. C. Morland, D. I. F. Grimes, and T. J. Hewison, "Satellite observations of the microwave emissivity of a semi-arid land surface," *Remote Sens. Environ.*, vol. 77, no. 2, pp. 149–164, 2001.
- [22] J. C. Morland, D. I. F. Grimes, G. Dugdale, and T. J. Hewison, "The estimation of land surface emissivities at 24 GHz to 157 GHz using remotely sensed aircraft data," *Remote Sens. Environ.*, vol. 73, no. 3, pp. 323–336, 2000.
- [23] J. R. Pardo, J. Cernicharo, and E. Serabyn, "Atmospheric Transmission at Microwave (ATM): An improved model for millimeter/submillimeter applications," *IEEE Trans. Antennas Propagat.*, vol. 49, no. 12, pp. 1683–1694, Dec. 2001.
- [24] C. Prigent, F. Chevallier, F. Karbou, P. Bauer, and G. Kelly, "AMSU-A land surface emissivity estimation for numerical weather prediction assimilation schemes," *J. Appl. Meteorol.*, 2005.
- [25] C. Prigent, J. Munier, G. Ruffié, and J. Roger, "Interpretation of passive microwave satellite observations over Oman and Egypt," presented at the *EGS-AGU*, Nice, France, 2003.
- [26] C. Prigent, J. P. Wigneron, B. Rossow, and J. R. Pardo, "Frequency and angular variations of land surface microwave emissivities: Can we estimate SSM/T and AMSU emissivities from SSM/I emissivities?," *IEEE Trans. Geosci. Remote Sensing*, vol. 38, no. 5, pp. 2373–2386, Sep. 2000.
- [27] C. Prigent, W. B. Rossow, and E. Matthews, "Global maps of microwave land surface emissivities: Potential for land surface characterization," *Radio Sci.*, vol. 33, pp. 745–751, 1998.
- [28] —, "Microwave land surface emissivities estimated from SSM/I observations," *J. Geophys. Res.*, vol. 102, pp. 21 867–21 890, 1997.
- [29] W. B. Rossow and R. A. Schiffer, "ISCCP cloud data products," *Bull. Amer. Meteorol. Soc.*, vol. 72, pp. 2–20, 1991.
- [30] F. Weng, L. Zhao, R. Ferraro, G. Poe, X. Li, and N. Grody, "Advanced microwave sounding unit cloud and precipitation algorithms," *Radio Sci.*, vol. 38, pp. 8.086–8.096, 2003.
- [31] F. Weng, B. Yan, and N. Grody, "A microwave land emissivity model," *J. Geophys. Res.*, vol. 106, no. D17, pp. 20 115–20 123, 2001.
- [32] J.-P. Wigneron, D. Guyon, J.-C. Calvet, G. Courrier, and N. Bruignier, "Monitoring coniferous forest characteristics using a multifrequency microwave radiometry," *Remote Sens. Environ.*, vol. 60, pp. 299–310, 1997.
- [33] A. J. Simmons and J. K. Gibson, "The ERA-40 Project plan," ECMWF, Reading, U.K., ERA-40 Project Report Series 1, 2000.

Fatima Karbou received the engineering degree in topography from the Institut Agronomique et Vétérinaire Hassan II, Rabat, Morocco, in 1999, and the Ph.D. degree in physics of remote sensing from Versailles Saint Quentin en Yvelines University, Vélizy, France, in 2004.

In September 2000 and during one year, she joined the ACRI research firm team at Sophia-Antipolis, France, as a Research Engineer. She worked on an air pollution simulator in both urban and rural environments and on NOAA instruments level 1 and 2 data processing tools. Her main fields of interest include the use of passive microwave instruments to estimate and analyze the land emissivities and to retrieve atmospheric parameters over land.